JOURNAL OF MATERIALS SCIENCE 35 (2000) 5169–5178

Morphology and mechanical property relationship in linear low-density polyethylene blown films

JIANJUN LU, HUNG-JUE SUE*
Polymer Technology Center, Department of Mechanical Engineering, Texas A&M University, College Station, TX 77843-3123, USA
E-mail: hjsu@acs.tamu.edu

THOMAS P. RIEKER
Center for Microengineered Materials, Department of Chemical and Nuclear Engineering, University of New Mexico, Albuquerque, NM 87131, USA

Linear low-density polyethylene (LLDPE) blown films fabricated under two different processing conditions, namely a non-stalk bubble configuration and a stalk bubble configuration, were investigated. Morphological characterization was performed using small-angle X-ray scattering, transmission electron microscopy, infrared dichroism, and differential scanning calorimetry. The findings on crystal orientation characteristics of the films suggest that modification on the widely accepted row orientation model of Keller and Machin may be needed. In comparison to the conventional non-stalk bubble geometry for LLDPE film blowing, the stalk bubble configuration can produce a more randomly orientated lamellar texture, resulting in less anisotropy in mechanical properties and a higher dart impact resistance. A good correlation between mechanical properties and morphological features was found.

1. Introduction

Polyethylene (PE) film is one of the most consumed polymeric materials today. Most PE films are produced by a tubular blowing process. In this process, polymer melt undergoes shear deformation inside a tubular die and the polymer chains reorientate themselves upon exiting from the die. Then, the tubular bubble is subject to a biaxial stretching, which is realized by stretching the bubble along the machine direction (MD) with a take-up device and along the transverse direction (TD) by bubble expansion. Fundamental processing-structure-property (P-S-P) relationships in PE blown films are important to blown-film manufacturers. Understanding of the P-S-P relationships will enable film manufacturers to predict the physical and mechanical properties of films and to determine the processing conditions and/or resin properties required for achieving certain film properties.

In the film blowing process, the primary molecular parameters are coupled with processing conditions to produce the final film morphology, which in turn determines the final film properties. Therefore, characterization of film morphology is crucial for establishing the fundamental P-S-P relationships. The study of the structure of PE blown films started in the 1950s. Holmes *et al*. [1] reported that the *a*-axis of the crystal unit cell lies along the extrusion direction in low-density polyethylene (LDPE) blown films. This finding was confirmed by Aggarwal *et al*. [2], who concluded that the crystallographic *a*-axis in PE blown film is orientated along the MD, while the *b*- and *c*-axes are randomly distributed in the plane perpendicular to the *a*-axis. Keller [3, 4] proposed the concept of row orientation in which the crystalline lamellar overgrowth occurs epitaxially from the *c*-axis orientated fibrils with radial growth in the *b*-direction and the *a*- and *c*-axes rotating about that growth direction. The resulting crystal orientation is that the *b*-axis has a preferred orientation perpendicular to the MD and the *a*- and *c*-axes are randomly distributed with cylindrical symmetry about the *b*-axis. Using the X-ray pole figure method for high-density polyethylene (HDPE) extruded films, Lindenmeyer and Lustig found support for the existence of row structure [5].

In 1967 Keller and Machin [6] gave a unifying picture and modified the row orientation model based on the level of stress for both LDPE and HDPE extruded films. They suggested that the row-nucleated structure is similar to the 'shish-kebabs' crystallized from a stirred solution. According to the modified model, two major crystallization processes take place depending upon the magnitude of the stress in the melt, namely "low-stress" and "high-stress" crystallizations. Under low-stress conditions, the lamellae grow

* Author to whom all correspondence should be addressed.

radially outward in the form of twisted ribbons, with the crystallographic *b*-axis parallel to their growth axis. As a result of this lamellar growth process, the *a*-axis of the crystal unit cell is orientated preferentially along the MD of the blown film. This texture is referred to as the Keller/Machin I morphology or a-texture. Under high-stress conditions, the radially grown lamellae extend directly outward without twisting. The folded chains (*c*-axis) within the lamellae remain parallel to the extended microfibers, resulting in the *c*-axis orientated preferentially along the MD. This is referred to as the Keller/Machin II morphology or c-texture. Intermediate stresses will lead to an incomplete twisting of the ribbons. This "row nuclei" model has been commonly used in the literature to describe the structures of PE blown films. The Keller/Machin I morphology is the most commonly observed morphology in PE blown films [7–15]. The Keller/Machin II morphology has been observed only in HDPE blown films [13, 16, 17].

In the 1970s, Maddams and Preedy published a series of papers based on an extensive texture investigation of very different HDPE blown films [12, 13, 16]. There were some maxima of orientation for the crystallographic *a*-, *b*-, and *c*-axes, which could be mainly connected with the types of stress crystallization. Notably, they found an additional orientation maximum of the *b*-axis in the normal direction (ND) connected with the transcrystalline portion of the material.

Choi *et al*. [14] used wide-angle X-ray scattering (WAXS), small-angle X-ray scattering (SAXS) and birefringence to characterize films fabricated under conditions ranging from uniaxial to biaxial extension, with concurrent measurements of the MD and TD stresses at the frost line. They proposed the presence of local lamellar stacks in HDPE blown films. The distribution of stack orientation is determined by the MD/TD stress balance at crystallization. White and Spruiell [18] developed a series of second-order moment biaxial orientation functions, which are useful for characterizing molecular orientation in films and sheets. Kwack and Han found that the biaxial stress ratio is the determining factor in the distribution of fibrillous nuclei and crystalline texture, as well as film anisotropy [15].

Previous investigations on PE blown films were mainly carried out on HDPE and LDPE. The blown films based on newly developed linear low-density polyethylene (LLDPE) give improved transparency and mechanical properties. Moreover, recent developments of new catalysts and processes enable producers to exercise a greater control over short chain branching distribution and molecular weight distribution. At this stage, no extensive morphological investigation has been performed on LLDPE blown films as were done on HDPE and LDPE.

As part of a larger effort to investigate P-S-P interactions in PE blown films, this study focuses on two LLDPE blown films made from the same LLDPE resin, but under different processing conditions. One film (Film A) was made using a conventional bubble geometry for LLDPE, i.e. a non-stalk bubble configuration. The other film (Film B) was blown using a stalk bubble configuration, which is typically employed for HDPE. Morphological investigation was carried out using transmission electron microscopy (TEM), infrared (IR) dichroism, SAXS, and differential scanning calorimetry (DSC). Morphological features were then correlated with the mechanical properties and processing conditions to understand the P-S-P relationships.

2. Experimental

2.1. Materials

Two LLDPE blown films (films A and B) were provided by Polyolefins Film Consortium at Texas A&M University. The resin used has a density of 922 kg/m^3 and a melt index of 0.22 g/10 min. The thickness of the films is about 25 μm. Film A was made using a conventional bubble geometry for LLDPE (i.e. a non-stalk bubble configuration), while film B was blown using a stalk bubble configuration. The processing parameters are listed in Table I.

2.2. Infrared dichroism

A Nicolet Avatar 360 Fourier Transform Infrared (FTIR) Spectrometer equipped with a polarizer was used to determine IR dichroism. The absorption bands at 730 and 719 cm^{-1} were employed to evaluate the orientations of crystal *a*-axis and *b*-axis, respectively. The band at 1368 cm^{-1} was used to evaluate amorphous orientation. The spectral separation procedure described by Kissin [19] was utilized to obtain the real absorbances from the measured absorbances of the bands. Dichroic ratio (D) was taken as the ratio of the absorbance measured with radiation polarized in the MD to that with radiation polarized in the TD. The method developed by Read and Stein [20] was used to calculate the orientation functions of f_a, f_b, f_c and f_{am}.

2.3. Transmission electron microscopy

Samples for TEM study were embedded in an epoxy and cured overnight at room temperature. The blocks were trimmed, faced-off, and then stained with RuO_4. Ultra-thin sections, ranging from 60 to 80 nm, were obtained using a Reichert-Jung Ultracut E microtome with a diamond knife. The thin sections were placed on 100-mesh Formvar-coated copper grids and examined using a Zeiss-10C TEM operating at an accelerating voltage of 100 kV.

2.4. Small angle X-ray scattering

The SAXS measurements were carried out at the University of New Mexico/Sandia National Laboratories SAXS laboratory [21]. Samples and backgrounds were run on a 5-m pinhole instrument in both long and short geometry configurations with

TABLE I Processing parameters for films A and B

Films	A	B
Die Gap (mm)	1.52	0.89
Melt Temperature (°C)	197	227
Blow Up Ratio	2.5	4
Draw Ratio	19.5	7.1
Output Rate (kg/h)	27	27

sample-to-detector distances of 2.48 m and 310 mm, respectively. When combined, the data sets span a q-range of $0.03 < q < 7.0$ nm^{-1}, where $q = 4\pi/\lambda \sin(2\theta/2)$. Here, λ is the wavelength of the radiation, and θ is the radial scattering angle. SAXS samples were prepared by carefully folding the blown films into 8 layers, and maintaining the MD of each layer parallel to every other. This produced samples with 0.20 mm in thickness. The samples were mounted on a sample changer such that the incident X-ray beam was normal to the plane of the films and that the machine direction (MD) was orientated in the beam with the same direction for all samples.

2.5. Differential scanning calorimetry

The DSC experiments were performed on a Perkin-Elmer Pyris-1 differential scanning calorimeter. Each experiment includes 3 steps: 1) temperature scan from -30°C to 180°C at a heating rate of 10°C/min; 2) cooling from 180°C to -30°C at a cooling rate of 20°C/min; and 3) repetition of step 1). A sample weight ranging from 7 to 10 mg was used. The weight percentage crystallinity of the PE films was obtained from DSC using 293 J/g as the heat of fusion of 100% crystalline PE [22].

2.6. Tensile tests

The engineering stress-strain curves and Young's moduli of the blown films were obtained by using a screw-driven mechanical testing machine (Instron, Model 1125) at ambient conditions. To obtain engineering stress-strain curves, specimens with dimensions of 50 mm × 12.7 mm (2″ × 0.5″) were stretched at a cross-head speed of 50 mm/min (2″/min) either to breaking or to the limit of the instrument. Young's moduli were determined by straining specimens with dimensions of 254 mm × 12.7 mm (10″ × 0.5″) sample at a cross-head speed of 25 mm/min (1″/min), following the ASTM D882-95a method.

3. Results and discussion

3.1. Morphological investigation

Fig. 1 shows the as-collected two-dimensional (2-D) SAXS pattern of film A, taken in long geometry. The presence of a preferred orientation of the lamellae within the sample is immediately evident from the anisotropic scattering pattern. The SAXS image of film B shows a similar pattern of the preferred orientation (not shown here). In such a 2-D image, the scattering angle 2θ is 0 at the center and increases with radius. The azimuthal angle, X, locates scattering features around the detector. X is set to zero at the 6 o'clock position of the detector plane and increases counter-clockwise. Regions of interest can be integrated over X or 2θ to produce intensity vs. 2θ or X data sets, respectively. The MD intercepts the detector at $X \cong 25^\circ$ and $205^\circ \pm 5^\circ$, i.e. along the line of scattering seen in Fig. 1. The intensity vs. X plots for the LLDPE films are shown in Fig. 2. From these plots, we can see that the long period lies along the MD in both LLDPE samples, i.e. the crystalline lamellae are orientated preferentially perpendicular to the MD. The full width at half height (FWHH) values derived from the plots in Fig. 2 are listed in Table II. The FWHH value for film A is about a third of that for film B, indicating a much higher degree of lamellar orientation in film A.

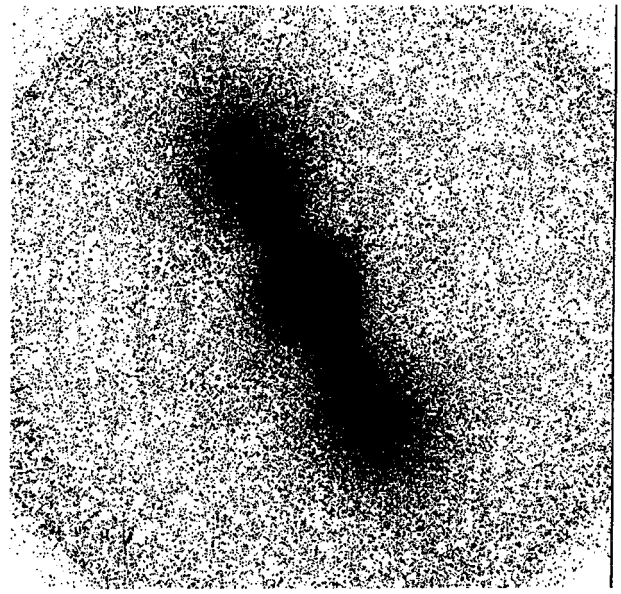

Figure 1 Two-dimensional SAXS image taken in long geometry for film A. The film is orientated perpendicular to the incident X-ray beam. Therefore, the image shows preferred orientation in the MD-TD plane of the sample.

TABLE II Selected morphological characteristics and mechanical properties of films A and B

Samples	Film A	Film B
FWHH (deg)	22	68
D_{730}	1.852	1.405
D_{720}	0.317	0.580
f_a	0.221	0.119
f_b	−0.294	−0.162
f_c	0.073	0.043
MD Young's Modulus (MPa)	275 ± 10	179 ± 7
TD Young's Modulus (MPa)	335 ± 6	169 ± 3
MD Elmendorf Tear (g)	14	81
TD Elmendorf Tear (g)	666	480
Dart Impact Resistance (g)	53	341

The IR dichroic ratios and the calculated orientation functions are listed in Table II. The orientation functions determined here give the averaged orientations of the crystal unit cell axes with respect to a reference direction, which is the MD in this case. In both films, the a-axis of the crystal unit cell is preferentially orientated along the MD, suggesting that the crystalline textures in films A and B agree with the a-texture. The absolute values of the a, b and c-axes orientation functions of film A are significantly bigger than those of film B, indicating that the crystallites in film A have higher degree of orientation than those in film B. The results of IR dichroism also suggest that the amorphous phase in both films has a slight preferential orientation along the MD. The amorphous orientation function of film A is significantly larger than that of film B.

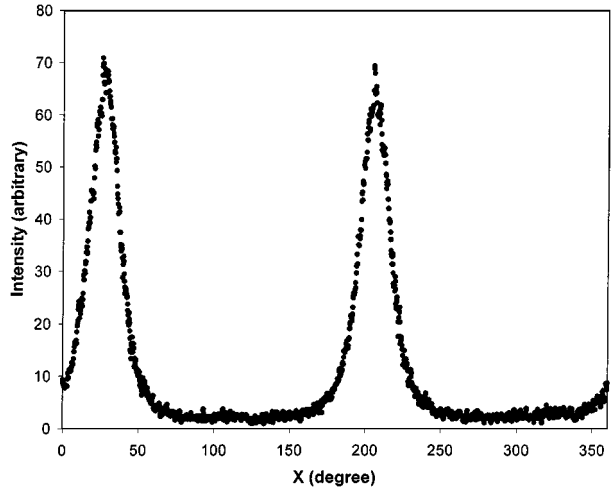

(a)

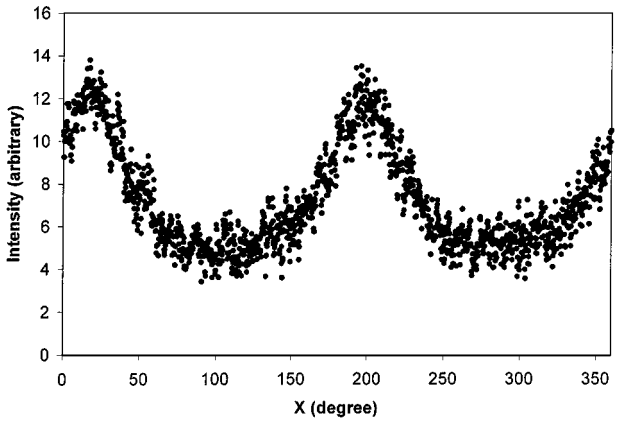

(b)

Figure 2 Intensity vs. X plots for (a) film A and (b) film B. The plots are generated by integrating two dimensional short-geometry SAXS data, over 2θ.

Figs 3 and 4 are TEM micrographs of films A and B, respectively. It is clear that film A possesses a significantly higher degree of lamellar orientation than film B. This finding is consistent with the SAXS and IR dichroism results. The TEM micrograph taken in the MD-ND plane shows that the lamellae in film A are well orientated with the lamellar normal along the MD (Fig. 3a). There are only few lamellae observed on the TEM micrograph taken in the TD-ND plane (Fig. 3b). Based on the TEM observations, it is evident that the lamellae in film A are predominantly orientated perpendicular to the MD.

IR dichroism results suggest that the crystalline texture of film A agrees with the a-texture. According to the row-nucleation model of Keller and Machin [6], the preferential *a*- and *c*-axes orientations along the MD in Keller/Machin I morphology (a-texture) are due to the twisting of lamellae along the lamellar growth direction (*b*-axis). However, no significant lamellar twisting can be observed in film A by TEM. The shape of the lamellae in this film is more like that described for the Keller/Machin II morphology (c-texture). The crystalline texture in this LLDPE film agrees with neither Keller/Machin I nor Keller/Machin II morphology. This may imply that lamellar twisting is not necessary for the formation of a-texture.

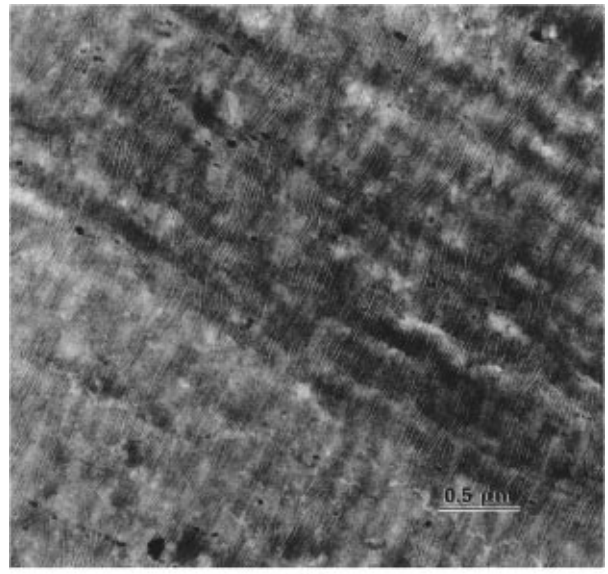

(a)

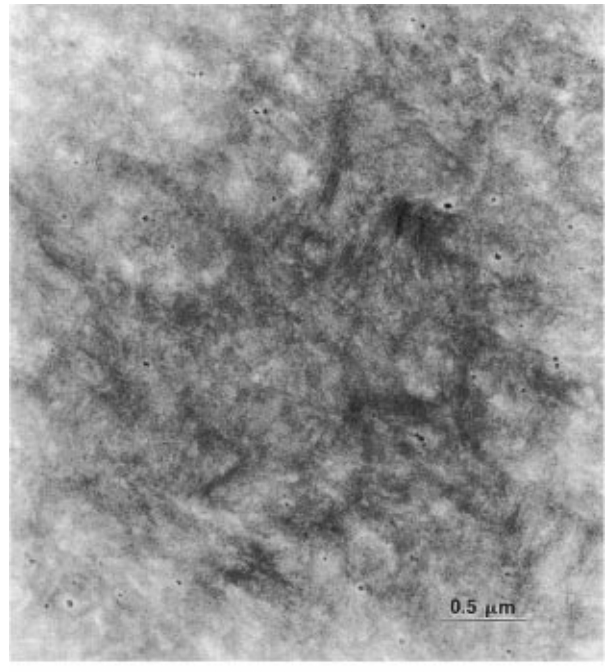

(b)

Figure 3 TEM micrographs of film A taken in (a) MD-ND plane and (b) TD-ND plane.

In the work of Keller and Machin [6], lamellar twisting was observed directly by TEM. In later investigations of blown film morphology, crystalline texture characteristics were usually determined by other techniques, such as X-ray diffraction, IR dichroism, etc. TEM was seldom used to examine the shape of lamellae. Experimental evidence has indicated that molecular chains can make an angle of up to 30° with the lamellar faces in some cases [23]. Given that the lamellae are

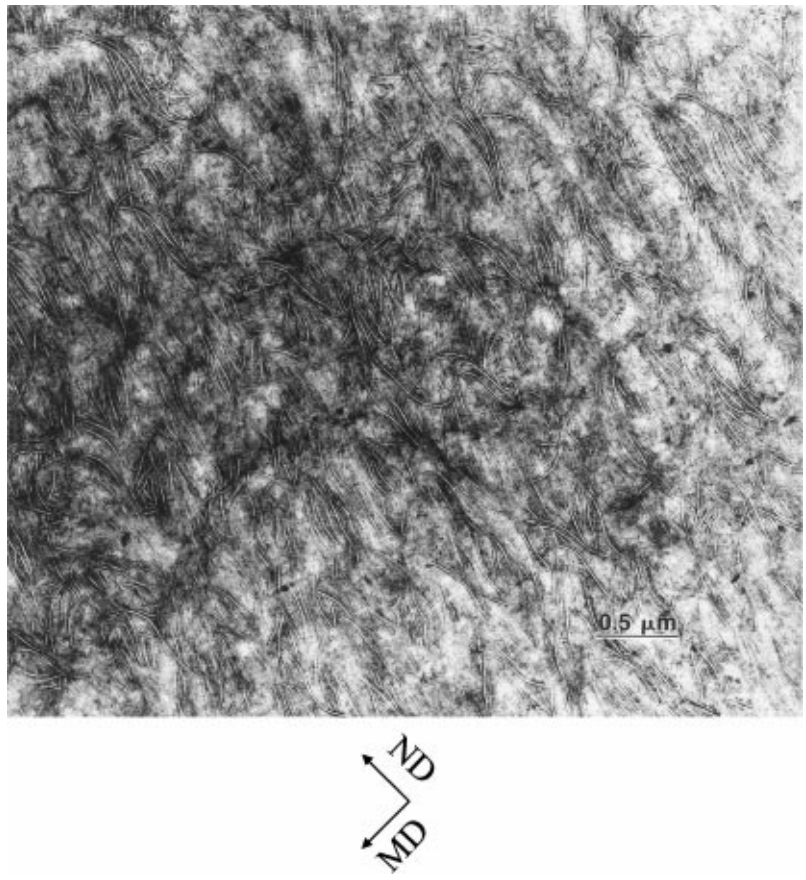

(a)

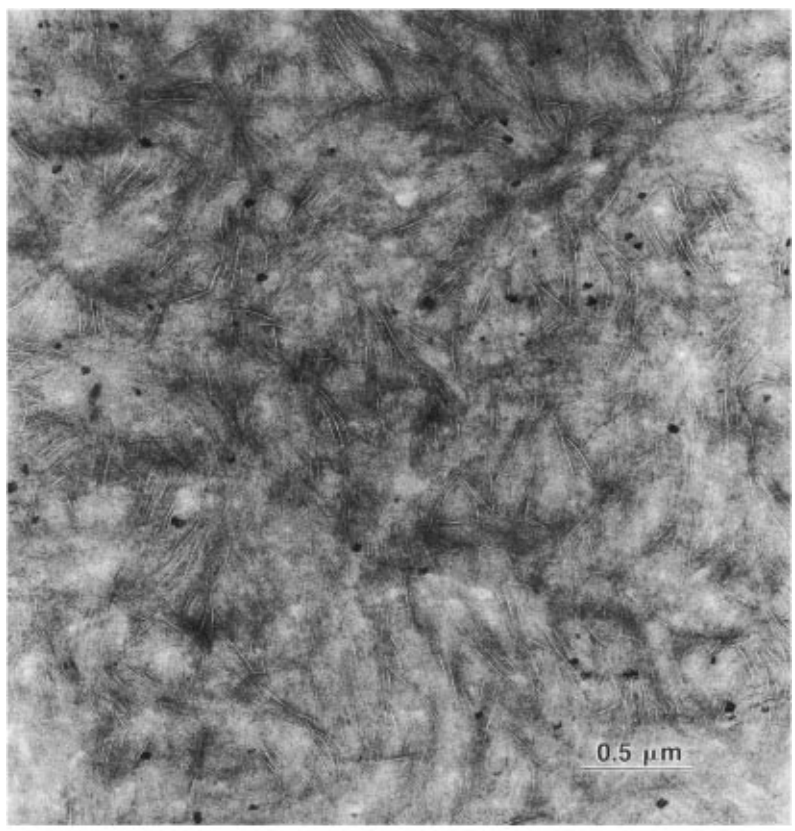

(b)

Figure 4 TEM micrographs of film B taken in (a) MD-ND plane and (b) TD-ND plane.

perpendicular to the MD in a film, the tilt of molecular chains relative to the lamellar normal will cause the *a*- and *c*-axes to orientate at an angle from the MD. Since the direction of chain tilt in a film is distributed in a cylindrical symmetry with respect to the machine direction in most cases, the overall result of the chain tilt will be that the orientation maxima of *a*- and *c*-axes are in the MD. Therefore, in theory, lamellar twisting is not necessary for forming the a-texture.

Lindenmeyer and Lustig [5] used WAXS pole figures for the characterization of *a*-, *b*- and *c*-axes orientations in LDPE and HDPE blown films. They found that the *a*-axis is in the MD but at an angle of approximately 65° to the plane of the film, and the *c*-axis distribution shows a maximum at about 45° to the plane of the film in the MD. The *b*-axis has a maximum in the TD. Choi *et al*. [14] observed that the *a*-axis is almost uniformly distributed around the MD, but exhibits maxima at about 47° to 61° away from the MD. In the above cases, both chain tilt and lamellar twisting could explain the experimental results. Since no TEM micrographs are available, it is hard to determine which is the main cause for such observations. Note that Choi *et al*. proposed that the films studied are biaxially orientated and contain local lamellar stacks. The distribution of stack orientation is determined by the MD/TD stress balance at crystallization. The orientation maxima of the crystallographic axes are the results of the distribution of lamellar stack orientation. In this complicated case, the shape of lamellae cannot be clarified without TEM study.

Another factor, i.e. transcrystallization, could also complicate the case. Transcrystalline material normally tends to have its *b*-axis orientated in the normal direction and *a*- and *c*-axes orientated in the plane of the film. Based on TEM, no significant amount of transcrystalline material is found near the surfaces of films A and B in this study.

In the TEM micrograph on the MD-ND plane (Fig. 4a), film B exhibits a rather random lamellar orientation. The cross-sections of many lamellae have a curved shape. A globally preferential lamellar orientation with the lamellar normal aligned in the MD is shown. Locally, both row-orientated superlamellar structures (Fig. 5) and highly disordered regions (Fig. 6) can be observed. Compared with film A, film B shows many more lamellae on the TD-ND plane micrograph (Fig. 4b). No preferred orientation or ordering of lamellae can be observed on the TD-ND plane for film B. Thus, TEM suggests that lamellar twisting may occur in film B. This further casts doubt about the necessity of lamellar twisting for the formation of the a-texture. According to the Keller/Machin model, film B should have a higher a-axis orientation than film A because of the lamellar twisting in film B, but IR dichroism shows the opposite.

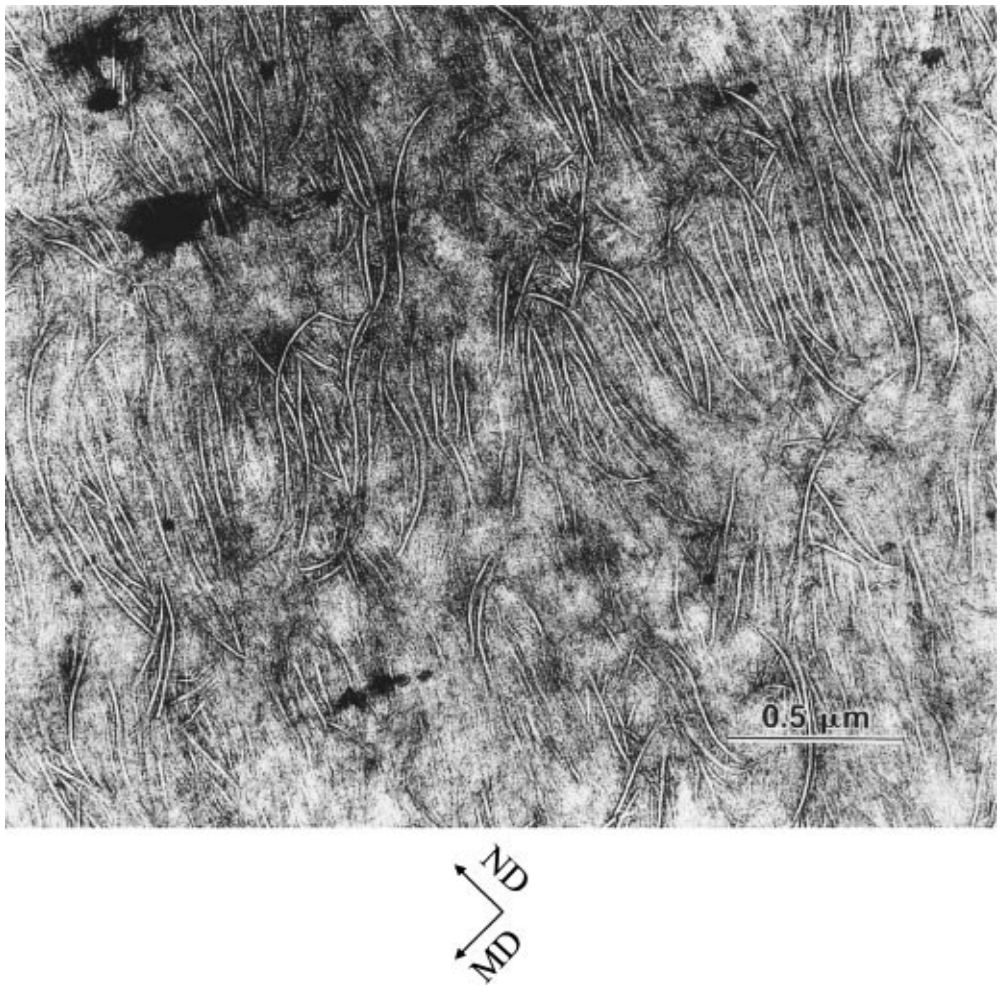

Figure 5 A TEM micrograph of film B taken in MD-ND plane.

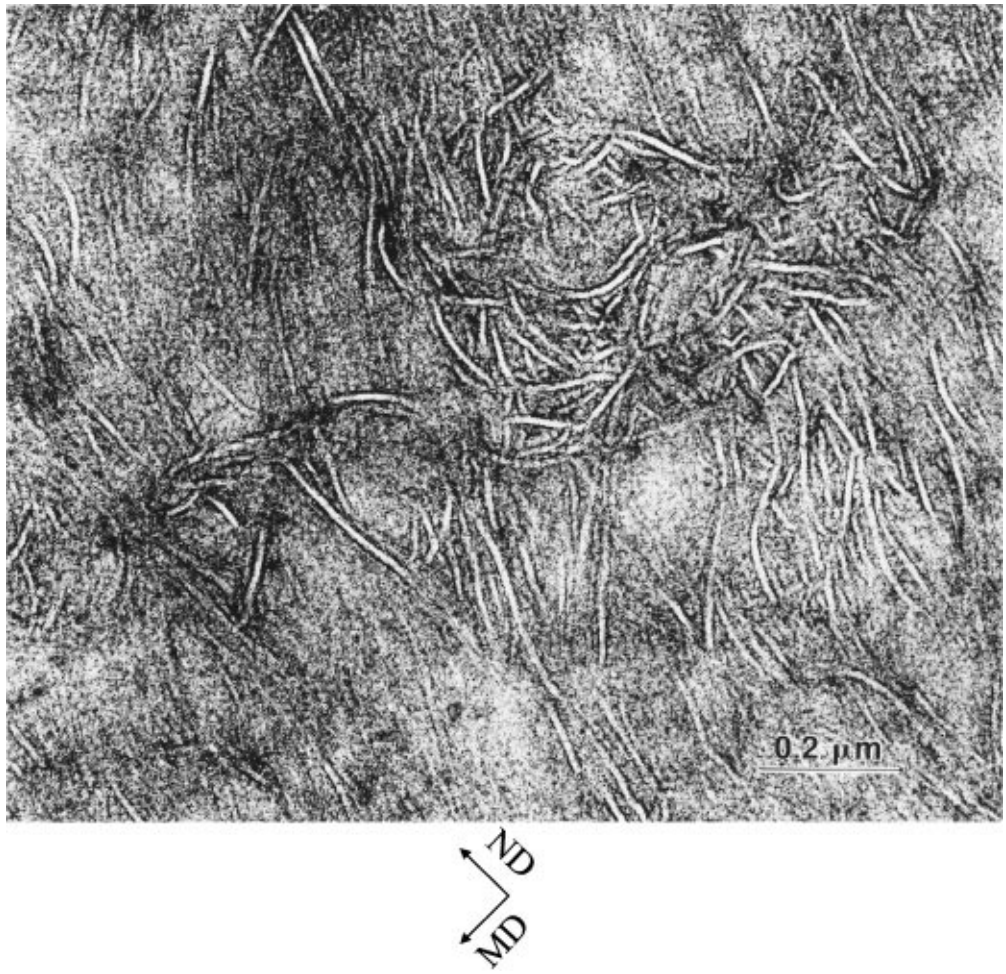

Figure 6 A TEM micrograph of film B taken in MD-ND plane.

The stalk bubble configuration is somewhat unusual for LLDPE film blowing as it is normally used for HDPE. The region between the die face and the stalk (bubble expansion zone) provides a region of low elongation rate in which a portion of the MD chain orientation introduced in the die can relax [24–26]. A higher stalk height gives a longer time for the chain orientation to relax, thus less MD orientation is "frozen" into the final blown films. The use of the stalk bubble configuration has another effect on the crystallization and orientation process. For this bubble configuration, the film blowing process is divided into two distinct deformation regimes [26], namely, a nearly planar extension in the stalk and a biaxial stretching in the bubble expansion zone. In the stalk region, a significant portion of MD stretching takes place, and the bubble diameter decreases (neck-in) [27]. Consequently, the magnitude of TD strain from the neck to the frost line can be much larger than the blow-up ratio, which is defined as the ratio of the film-tube diameter at the frost line to the extrusion die diameter. These factors may contribute to the more random lamellar orientation in film B. Furthermore, it should be noted that the lower draw ratio, higher blow-up ratio, higher melt temperature, and smaller die gap are also contributing factors for the lower lamellar orientation in film B [28].

In the DSC experiments, the crystallinities of the two films were found to be the same, i.e. 46% by weight. For each film, several independent DSC tests were performed. It was found that the shape of the melting peak for the first temperature scan varies significantly from test to test, although the heat of fusion stays constant. After the specimen was cooled to -30°C again, the second temperature scan was performed. The second scans produce melting peaks with the same shape in all tests for both films (Fig. 7). This is because the thermal history in the original films was eliminated upon the first melting. The results of the second scans indicate that the variation of the melting peak shape upon the first temperature scan is not an experimental uncertainty. The morphology is not uniform in the blown films studied. However, it is interesting to note that each of these melting peaks seems to be composed of two overlapping peaks with different peak temperatures. The magnitudes of these two peaks vary, but the sum of the two is relatively constant. A DSC profile (heat flow versus temperature) can be converted into a lamellar thickness distribution curve (relative probability of the weight percentage of lamellae versus lamellar thickness) by using the Gibbs-Thomson equation [29]. The lamellar thickness distribution curves of the two films are shown in Fig. 8. It is obvious that there exists a bimodal lamellar thickness distribution in both films. This bimodal lamellar thickness distribution is confirmed by the lamellar thickness measurement on the TEM micrographs (Fig. 9). The cause

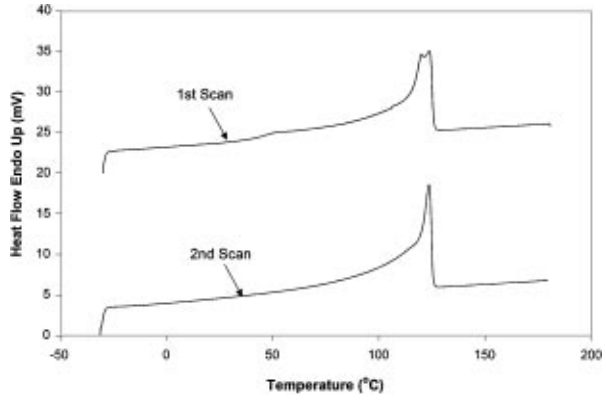

(a)

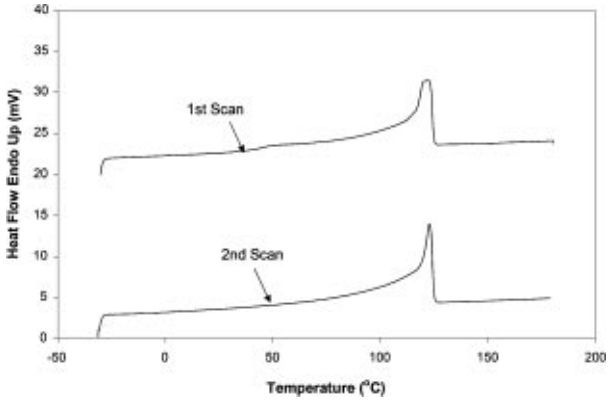

(b)

Figure 7 DSC thermographs of (a) film A and (b) film B.

for this bimodal lamellar thickness distribution is still unclear.

3.2. Structure-property relationship

The engineering stress-strain curves of the LLDPE films are shown in Fig. 10. For film A, the TD stress-strain curve shows a sharp "conventional" yield peak. The yielding is followed by necking (observed during testing) and a cold-drawing process. The cold-drawing process continues until all "fresh" material between the two grips is cold-drawn. Eventually, strain hardening occurs. In the MD tensile test of film A, strain hardening occurs right after yielding. No necking is observed. On the contrary, the tensile behaviors of film B in the MD and TD are much more similar to each other. Strain hardening occurs in both MD and TD, but exhibiting a smaller magnitude than that observed in the MD for film A. In the MD, strain hardening occurs earlier and at a higher stress level.

Semicrystalline polymers can be considered as consisting of crystalline lamellae held together by tie chains and separated by an amorphous phase. When these polymers are stressed, what occurs first is the deformation at the crystalline lamella and amorphous layer level. Three deformation modes, namely lamellar separation, lamellar shear and lamellar rotation, can be postulated at this structural level [30]. Since the lamellae are held together by tie chains, these lamellar displacement motions are restricted to a small magnitude before

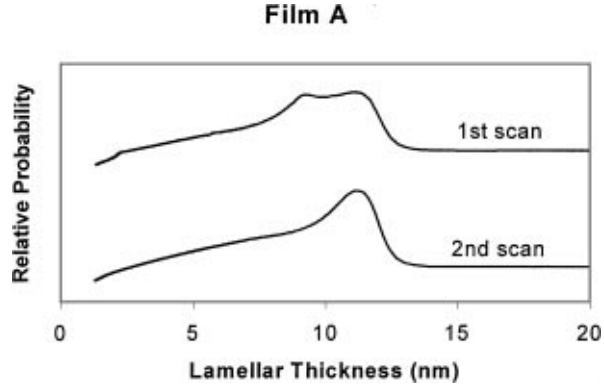

(a)

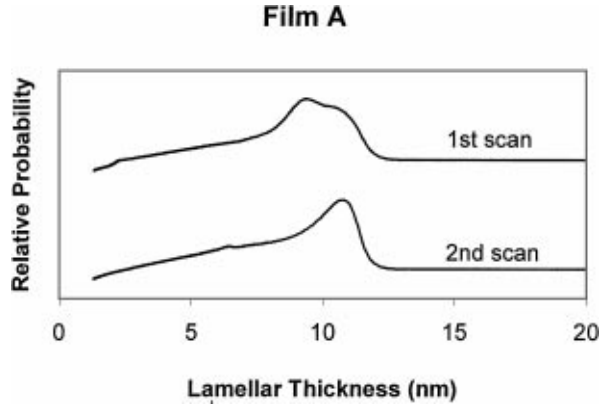

(b)

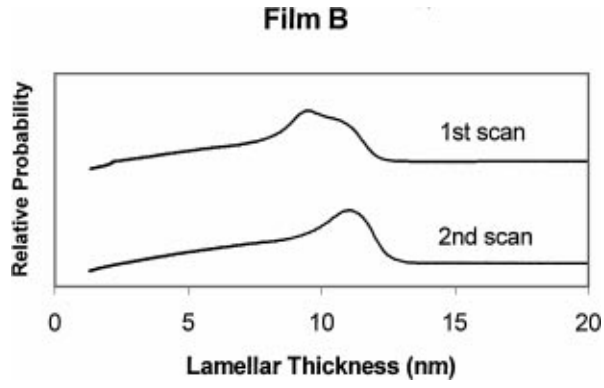

(c)

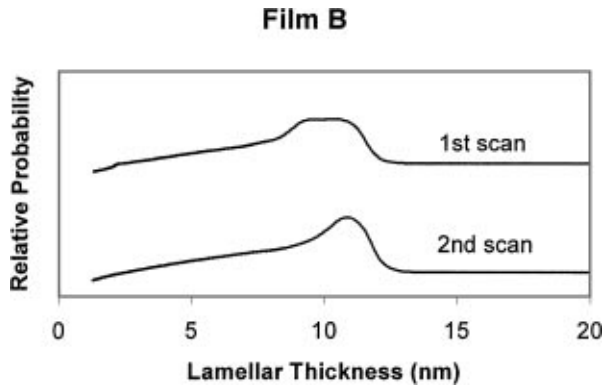

(d)

Figure 8 Lamellar thickness distribution curves obtained from DSC: (a) and (b) are from two independent tests on Film A; (c) and (d) are from two independent tests on Film B.

the disruption of crystalline lamellae at the crystallographic level occurs. The deformation mechanisms at the crystallographic level may involve chain slip and transverse slip, mechanical twinning, martensitic phase

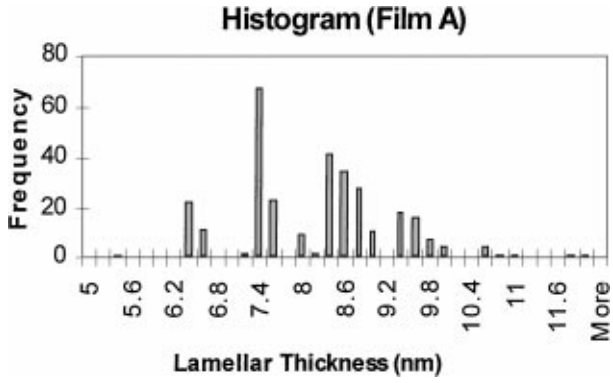

(a)

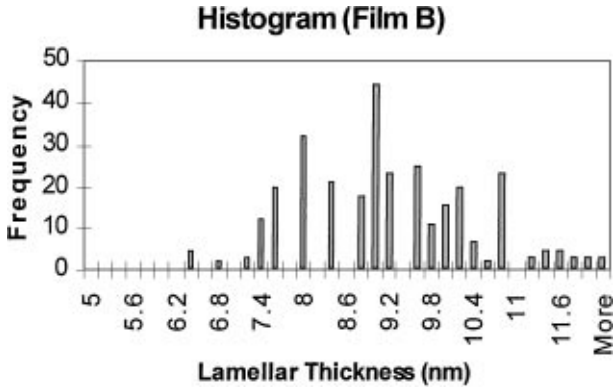

(b)

Figure 9 Lamellar thickness distribution histograms obtained from TEM micrographs for (a) film A and (b) film B.

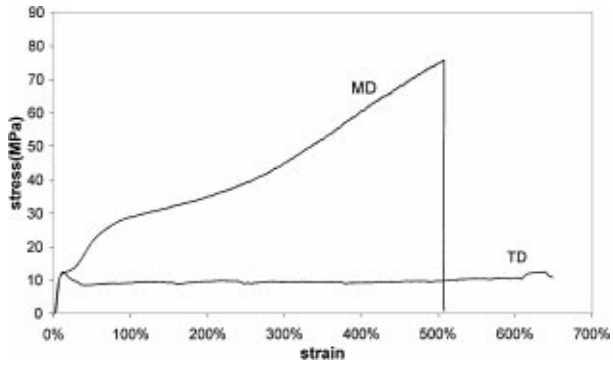

(a)

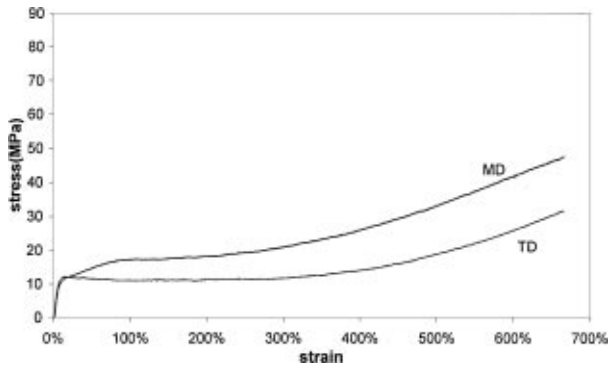

(b)

Figure 10 Engineering stress-strain curves of (a) film A and (b) film B.

transformation, decrystallization and recrystallization processes [30–33].

In film A, lamellae are stacked with normals more or less aligned along the MD. When it is stretched along the MD, lamellar separation is the dominant deformation mechanism at first. However, the extent of the separation will be limited due to the existence of tie chains. Upon further stretching, the crystalline lamellae have to deform to allow higher straining. This results in the yielding of the film. When film A is stretched along the TD, the deformation at the level of the crystalline lamella and amorphous layer, i.e. lamellar separation, lamellar shear and lamellar rotation, is largely limited. As a result, the film yields at a small magnitude of strain. In the MD stretching, chain slip is the dominant deformation mode of the crystalline phase following yielding. On the contrary, the break-up of the crystalline lamellae, the pull-out of the chains from the lamellae and transverse slip are the major deformation mechanisms of the crystals in TD stretching. The pull-out of polymer chains in this case is perpendicular to the lamellar normal. It is clear that the pull-out of chains in this direction is much easier than that in the chain slip, and is basically a cold-drawing process. Therefore, there is a long horizontal plateau on the stress-strain curve for the TD stretching, while strain hardening occurs in the MD stretching of this sample. Since film B has a more random lamellar orientation, the tensile behaviors in the MD and TD are similar to each other. Compared with film A, more lamellar shear and lamellar rotation are involved in the MD and TD stretching of film B.

The stress-strain curves for the MD stretching of both films show a double yielding phenomenon. The two yield points have been speculated to originate from lamellar shear and the subsequent deformation of the crystalline phase [34, 35]. The yield stress at the second yield point of film A is much higher than that of film B, probably due to a greater degree of lamellar stacking along the MD in film A.

The tear strengths and dart impact resistances of the LLDPE blown films studied were provided by the manufacturers, and are listed in Table II. From Table II, we can see a much higher Elmendorf tear strength in the TD than in the MD for both films due to the preferred lamellar orientation in the films. As the degree of preferred lamellar orientation in film B is lower, the difference between the tear strengths in the MD and TD of film B turns out to be smaller. This may be the reason why film B has a higher dart impact resistance than film A, since the dart drop impact resistance is commonly recognized to be related to the balance of mechanical properties between the MD and TD [36].

Young's modulus of semicrystalline polymers is governed by crystallinity, crystalline and amorphous phase orientation. Provided that two films have the same crystallinity, it is usually expected that if one film has a higher modulus in the MD, it should have a lower modulus in the TD [37, 38]. In this study, film A has a significantly higher modulus than film B in both the MD and TD, although the DSC study shows they have the same crystallinity (Table I). There are two possible reasons for this finding. First, film A has a greater amorphous phase orientation along the MD than film B. Secondly, the two-phase model for semicrystalline polymers (i.e. semicrystalline polymers consist of crystalline and amorphous phases) is not sufficient to describe the detailed structure of semicrystalline polymers [39–45].

Preliminary results from the solid-state NMR study indicate that there is a significant amount of noncrystalline interfacial component between the crystalline and amorphous phases in LLDPE blown films. Films A and B appear to have significantly different amounts of crystalline and interfacial phase contents, although they have almost the same amount of amorphous material. Film A has a higher crystalline content and a lower interfacial content than film B. This fact may contribute to the higher modulus of film A. Further solid-state NMR study of PE blown films is underway and the results will be published in a separate paper.

4. Conclusion

In the LLDPE blown films investigated, the lamellae were found to be preferentially orientated perpendicular to the MD. The degree of orientation is significantly affected by processing conditions. Compared with the conventional non-stalk bubble geometry for LLDPE blown films, the stalk bubble configuration can give a more random lamellar texture and more balanced mechanical properties. For the film produced by the non-stalk bubble configuration, the orientation distribution of crystal unit cells agrees with the typical Keller/Machin I morphology, but the shape of the lamellae agrees with the typical Keller/Machin II morphology. This suggests that the row orientation model of Keller and Machin may need modification. It also implies that lamellar twisting may not be necessary for the formation of a-texture. A good correlation between mechanical properties and morphological features is found.

Acknowledgements

The authors would like to thank the Polyolefins Films Consortium (Equistar Chemical Company, Exxon Chemical Company, Phillips Petroleum Company, Texas Eastman Chemical Company and Union Carbide) at Texas A&M University for financial support and providing the PE blown films. Financial support from National Science Foundation (grant number: NSF/CTS-9705467) and the instrument funding from the South Texas Section of SPE are also greatly appreciated. Special thanks to E. I. Garcia-Meitin and Helga Sittertz-Bhatkar for their valuable aid with the TEM work. Thomas Rieker acknowledges financial support from Sandia National Laboratories operated for the U.S. Department of Energy under contract number DEAC04-99AL85000.

References

1. D. R. HOLMES, R. G. MILLER, R. P. PALMER and C. W. BUNN, *Nature* **171** (1953) 1104.
2. S. L. AGGARWAL, G. P. TILLEY and O. J. SWEETING, *J. Appl. Polym. Sci.* **1** (1959) 91.
3. A. KELLER, *Nature* **174** (1954) 826.
4. *Idem., J. Polymer Sci.* **15** (1955) 31.
5. P. H. LINDENMEYER and S. J. LUSTIG, *J. Appl. Polym. Sci.* **9** (1965) 227.
6. A. KELLER and M. J. MACHIN, *J. Macromol. Sci.* **B1** (1967) 41.
7. C. R. DESPER, *J. Appl. Polym. Sci.* **13** (1969) 169.
8. K. KOBAYASHI and T. NAGASAWA, *J. Polym. Sci: Part C* **15** (1966) 163.
9. J. M. HAUDIN, *Ann. Chim. Fr.* **5** (1980) 513.
10. H. ASHIZAWA, J. E. SPRUIELL and J. L. WHITE, *Polym. Eng. Sci.* **24** (1984) 1035.
11. E. WALENTA, A. JANKE, D. HOFMANN, D. FANTER and D. GEISS, *Acta Polym.* **37** (1986) 557.
12. W. MADDAMS and J. PREEDY, *J. Appl. Polym. Sci.* **22** (1978) 2721.
13. *Idem., ibid.* **22** (1978) 2738.
14. K. CHOI, J. E. SPRUIELL and J. L. WHITE, *J. Polym. Sci., Polym. Phys. Ed.* **20** (1982) 27.
15. T. H. KWACK, C. D. HAN and M. E. VICKERS, *J. Appl. Polym. Sci.* **35** (1988) 363.
16. W. MADDAMS and J. PREEDY, *ibid.* **22** (1978) 2751.
17. T. H. YU and G. L. WILKES, *Polymer* **37** (1996) 4675.
18. J. L. WHITE and J. E. SPRUIELL, *Polym. Eng. Sci.* **21** (1981) 859.
19. Y. V. KISSIN, *J. Polym. Sci., Polym. Phys. Ed.* **30** (1992) 1165.
20. B. E. READ and R. S. STEIN, *Macromolecules* **1**(2) (1968) 116.
21. T. P. RIEKER and P. F. HUBBARD, *Rev. Sci. Inst.* **69** (1998) 3504.
22. L. MANDELKERN, "Crystallization of Polymers" (McGraw Hill, New York, 1964).
23. F. KHOURY and L. H. BOLZ, in 38th Annual Proceedings of the Electron Microscopy Society of America, San Francisco, California, edited by G. W. Baily (Claitors, Baton Rouge, 1980) p. 242.
24. H. H. WINTER, *Pure and Appl. Chem.* **55** (1984) 943.
25. T. KANAI, M. KIMURA and Y. ASANO, *J. Plastic Film and Sheeting* **2** (1986) 224.
26. P. P. SHIRODKAR and S. D. SCHREGENBERGER, in Proceedings of the 45th Society of Plastics Engineers Annual Technical Conference (ANTEC), Los Angeles, May 1987, p. 37.
27. E. J. DORMIER, J. M. BRADY, W. H. CHANG, S. D. SCHREGENBERGER and J. D. BARNES, in Proceedings of the 47th Society of Plastics Engineers Annual Technical Conference (ANTEC), New York, May 1989, p. 696.
28. T. H. YU and G. L. WILKES, *J. Rheol.* **40** (1996) 1079.
29. J. D. HOFFMAN, "Treatise on Solid State Chemistry, Vol. 3." (Plenum Press, New York, 1976).
30. P. B. BOWDEN and R. J. YOUNG, *J. Mater. Sci.* **9** (1974) 2034.
31. L. LIN and A. S. ARGON, *ibid.* **29** (1994) 294.
32. D. M. SHINOZAKI and G. W. GROVES, *ibid.* **8** (1973) 1021.
33. I. L. HAY and A. KELLER, *J. Polym. Sci.* **30** (1970) 289.
34. N. W. BROOKS, R. A. DUCKETT and I. M. WARD, *Polymer* **22** (1992) 1975.
35. N. W. BROOKS, A. P. UNWIN, R. A. DUCKETT and I. M. WARD, *J. Macromol. Sci.* **34** (1995) 29.
36. Y. KIM, C. KIM, J. PARK, C. LEE and T. MIN, *J. Appl. Polym. Sci.* **63** (1997) 289.
37. D. M. SIMPSON and I. R. HARRISON, *J. Plastic Film & Sheeting* **10** (1994) 302.
38. H. ZHOU and G. L. WILKES, *J. Mater. Sci.* **33** (1998) 287.
39. K. BERGMANN, K. NAWOTKI and Z. Z. KOLL, *Polymer* **219** (1967) 132.
40. *Idem., ibid.* **251** (1973) 962.
41. R. KITAMARU, F. HORII and S.-H. HYON, *J. Polym. Sci., Polym. Phys.* **15** (1977) 821.
42. R. KITAMARU and F. HORII, *Adv. Polym. Sci.* **26** (1978) 139.
43. G. R. STROBL and W. J. HAGEDORN, *J. Polym. Sci., Polym. Phys.* **16** (1978) 1181.
44. L. MANDELKERN, *Acc. Chem. Res.* **23** (1990) 380.
45. *Idem., Chemtracts: Macromol. Chem.* **3** (1992) 347.

Received 18 January
and accepted 22 February 2000